JOURNAL OF THEORETICAL
AND APPLIED MECHANICS
63, 2, pp. 415–430, Warsaw 2025
https://doi.org/10.15632/jtam-pl/202022

CREEP TEST AND CONSTITUTIVE MODEL FOR GRANITE WITH DIFFERENT WATER CONTENT AFTER HIGH TEMPERATURE COOLING

Guang-Chao ZHANG[1,2], Zhao-Teng JI[1,2], Jun-Yan SU[1], Wu-Kui DAI[1], Jian-Jun YANG[1,2*]

[1] *China Northeast Architectural Design & Research Institute Co., Ltd, Shenyang 110055, Liaoning, China*
[2] *ZJDS Geotechnical Engineering Co., Ltd, Shenyang 110055, Liaoning, China*

*corresponding author, *jianjunyang147@163.com*

Granite was selected as the test specimen to carry out the rock triaxial compression creep test under different water content after high temperature cooling. The creep rate at low stress levels includes deceleration creep rate and steady creep rate. The new damage variable can not only describe the physical damage of the crack growth under the action of temperature, but also characterize the mechanical damage of the specimen under the action of loading. A new damage creep model was obtained by modifying the Burgers model. The research can provide ideas for the support of a high and steep slope.

Keywords: high temperature; water content; granite; high and steep slope; damage model.

1. Introduction

Minerals are one of the important resources in the world, which is related to the long-term development and security of a country (Diederichs *et al.*, 2004). The problem of open-pit slope directly affects the economic benefit of open-pit mining and the safety of production (Abbas *et al.*, 2023; Bandis *et al.*, 1983). Open-pit slope excavation has the following characteristics:

- the construction objects of high and steep open-air slopes were mainly granite, igneous rock or metamorphic rock, whose compressive strength was generally above 80 MPa;
- the ambient temperature of deep-buried rock was generally higher than 100°;
- the deep buried rock mass near the water table in the high and steep open-air slope was often affected by the high temperature and groundwater, resulting in the rock mass failure and further affecting the stability of the slope.

Therefore, the study of rock mechanical properties after high temperature cooling is of great significance for slope stability research.

In resource exploitation and underground engineering construction, it is inevitable to encounter a high temperature environment (Diederichs *et al.*, 2004). For example, the development and utilization of high-temperature rock mass, deep underground disposal of high-level nuclear waste, deep mining of mine rock mass, underground coal gasification, stability of the surrounding rock wall of ultra-deep drilling and other related rock mechanics engineering all involve the influence of high temperature on rock. Uniaxial compression tests were carried out on shale samples with different bedding angles after heat treatment at different temperatures. Acoustic emission monitoring was used to analyze crack propagation. Uniaxial compressive strength tests of sandstone at different temperatures were carried out to explore the mechanical response of sandstone to significant temperature changes (Ranjith *et al.*, 2012). The above research mainly analyses the physical and mechanical properties of rocks from the perspective of temperature,

but does not consider the damage and failure of rocks under the coupling effect of temperature and water.

Research and analysis of rock damage characteristics under different factors were mainly conducted through damage models. To describe the damage degree of physical and mechanical properties of granite after natural cooling at a high temperature treatment and the impact of a high temperature treatment on physical and mechanical properties of rock, research on damage variables by domestic and foreign scholars mainly include: mass damage variable $D(m)$ (Lin *et al.*, 2022), volume damage variable $D(v)$ (Liu *et al.*, 2020b), density damage variable $D(\rho)$ (Ahmed *et al.*, 2020), longitudinal wave velocity damage variable $D(P)$ (Gao *et al.*, 2020), porosity damage variable $D(\Phi)$ (Cao *et al.*, 2024), uniaxial compressive strength $D(\mathrm{UCS})$ (Shao *et al.*, 2022), and shear modulus damage variable $D(G)$ (Hamdi *et al.*, 2011) were used as heat treatment damage parameters. The above studies lack the analysis of rock damage model under the coupling effect of water content and temperature.

In the deep formation environment of a high and steep slope, rock was often in the alternating environment of high temperature and cold water, so it was necessary to study the damage and fracture of rock formation. In this study, the triaxial compression creep test of granite with different water content under high temperature cooling was carried out. The creep characteristics, damage variables and failure modes were analyzed, and the damage index of rock at a high temperature and water content was mainly analyzed. Aiming at the deficiency of a single damage variable, a new coupled damage index was constructed to characterize the comprehensive damage characteristics. Based on the component combination theory, a new damage rheological model describing the whole process of rock creep was obtained by connecting the accelerating element with the Burgers model describing the decay and stability stages of rock. The model has the advantages of fewer parameters and accurate calculation. The research can also provide theoretical support for the stability analysis of high and steep open-air slopes.

2. Test procedures and methodology

2.1. Rock material and test specimen

The study site was selected from the slope of the Huabei granite open pit in Hunyuan County, Shanxi Province, and the granite samples were prepared according to the standards of the International Association of Rock Mechanics (Peellage *et al.*, 2024). The sample is a cylinder with a diameter of 50 mm and a height of 100 mm, the end surface roughness is less than 0.5 mm (Fig. 1a). There are four main water-bearing states of deep rock mass samples: dry state, natural state, natural water-saturated state, and fully water-saturated state. The production process of samples with different water content states is as follows:

- dry state specimen: the drying test is to obtain the rock sample without water. The specimen is placed in the drying box at 100° for 24 h, weighed after taking it out, and then placed in the drying box again for heating and weighing again. If the weight does not change, the drying test ends; if the weight changes, the drying test continues until the weight of the rock sample does not change;
- natural state specimen: the raw rock specimen is cut according to the above size;
- natural saturated state specimen: the specimen was immersed in pure water, the specimen was taken out after 24 h, the surface moisture was wiped with a wet towel, and it is still put back in the water container after weighing, and then weighed once every 24 h until the quality difference between the two times does not exceed 0.01 g;
- fully saturated state specimen: the specimen is placed in a vacuum saturated water instrument and weighed every 24 h until the mass difference between the two is within 1 %. The results show that the water content of dry, natural, naturally saturated and fully saturated granite specimens is 0, 0.5 %, 1.0 %, and 2.0 %, respectively.

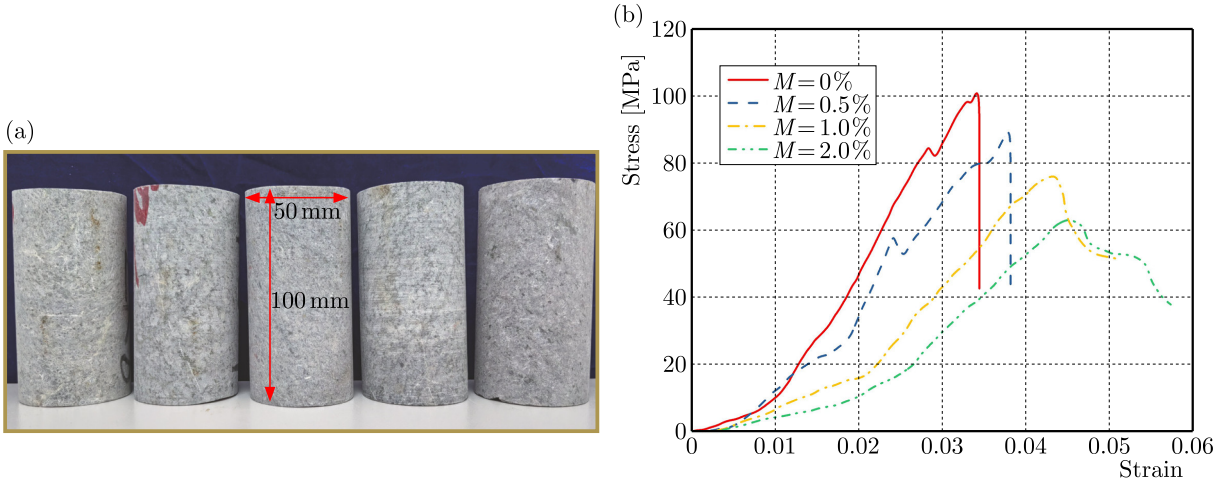

Fig. 1. (a) Granite specimen; (b) stress-strain curves of rocks with different water content.

To determine the stress level of granite creep test under different water content, uniaxial compression tests were carried out on specimens with different water content, as shown in Fig. 1b.

When the water content is low ($M = 0\,\%$ and $M = 0.5\,\%$), due to no water filling or less water filling in the initial pores of the granite, the bonding between the sample particles is strong, resulting in the deformation of the granite sample in the pre-peak stage is almost linear elastic, without obvious plastic deformation, showing significant brittle failure. In the naturally saturated state ($M = 1.0\,\%$), the compaction stage of the granite sample is relatively long, and before the peak stress, due to the water entering the pores of the specimen, the bonding between the particles is weakened, and the specimen has a significant plastic deformation, this has been verified by relevant literature (Liu *et al.*, 2020a). In the failure stage after the peak, the stress-strain curve shows a stepped stress drop. When the water content is high ($M = 2.0\,\%$), the weakening effect of water is the most obvious in the whole deformation and failure process, which makes the deformation of the granite sample larger. The stress-strain curve is convex shortly after loading, and the duration of the linear elastic deformation stage is relatively short. In the pre-peak stage, there is significant plastic deformation, and even a yield platform appears in the completely saturated state. In addition, the density, longitudinal wave velocity, elastic modulus and tensile strength of the granite are $2.592\,\mathrm{g\cdot cm^{-3}}$, $3260\,\mathrm{m\cdot s^{-1}}$, 46.5 GPa, and 5.42 MPa, respectively. In this experiment, the longitudinal wave velocity of rock was measured by the ZT801 rock mass parameter tester.

2.2. Experimental setup and test plan

The stress level and stress state of rock in the deep rock mass are different from that of rock in the surface layer. To make the test conditions more realistic, the test scheme is set from the mechanical state of rock and the occurrence conditions of confining pressure, high temperature and water content are considered. The test equipment used mainly includes:

- rapid heating box type electric furnace, which can perform high temperature heat treatment of the specimen, the maximum heating temperature of the equipment can reach 1600°, and the temperature control accuracy is 1°;
- vacuum water filling device, the device is mainly used for vacuum water filling treatment of granite specimens, in which the pumping rate is 1 l/s, the limit vacuum is 6×10^{-2} Pa, and the vacuum pump power is 150 W;
- the test equipment used was the MTS815.02 rock test system. Its maximum confining pressure was 100 MPa, and the precise range of force measurement was $-1\,\%\sim+1\,\%$.

The triaxial creep test steps of granite under different water content after high temperature cooling are shown as follows (Fig. 2): first of all, the horse boiler was used for high temperature heat treatment of granite samples, the temperature control rate is 5 °/min, and when it reaches 200°, it is maintained at a constant temperature for 24 h, and then the power supply of the heating furnace was turned off, so that the rock samples were naturally cooled to normal temperature in the furnace. The research object is the slope of the west side of the North China open-pit mine. The open-pit mine was mined to 1850 m, and the formation temperature was about 200°. Therefore, 200° was selected as the temperature of the test specimen. Then, the method in Subsection 2.1 was adopted to treat the granite specimens cooled at high temperature with different water content. The water content of the specimens was mainly obtained by calculating the mass of the specimens before and after filling with water. Finally, the triaxial creep test was carried out on the specimen. First, the granite specimen after the above treatment was sealed and placed in the triaxial compression test instrument. Then the confining pressure value of 30 MPa was applied at the loading rate of 0.5 MPa/min and kept stable, and finally the axial load was applied step by step until the specimen was damaged. The granite in the stratum slope environment was in the high ground stress environment, and the deep rock body was subjected to the vertical stress caused by the overlying rock body weight and the tectonic stress caused by the surrounding geological environment (Lemaitre, 1985). Considering the granite density and sampling depth, the triaxial compression confining pressure was 30 MPa, while the axial stress level was obtained by dividing the peak stress into five grades.

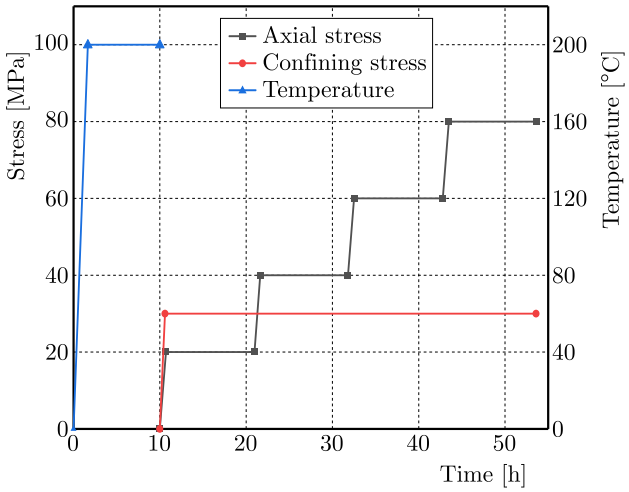

Fig. 2. Stress path.

3. Analysis of test results

3.1. Creep curve

Under the action of external force, the granite sample was compressed in the step creep test, and the tiny cracks and defects among the crystal particles in the sample due to the action of high temperature were further expanded. The low stress level will cause the internal cracks of the specimen to be crowded and closed. Under the action of external forces, the specimen will produce elastic deformation in a short time and gradually stabilize. This process takes a relatively small amount of time, but it is an important stage for the initiation of microcracks in the specimen. With the gradual stability of the internal stress distribution, the specimen enters the creep deformation stage (Fig. 3). At high stress levels, the specimen mainly deforms non-uniformly, which is manifested in two parts: on the one hand, the displacement dominated by high temperature, which is embodied in the expansion of macroscopic cracks. On the other hand, the pore water pressure further increases the crack expansion rate under load.

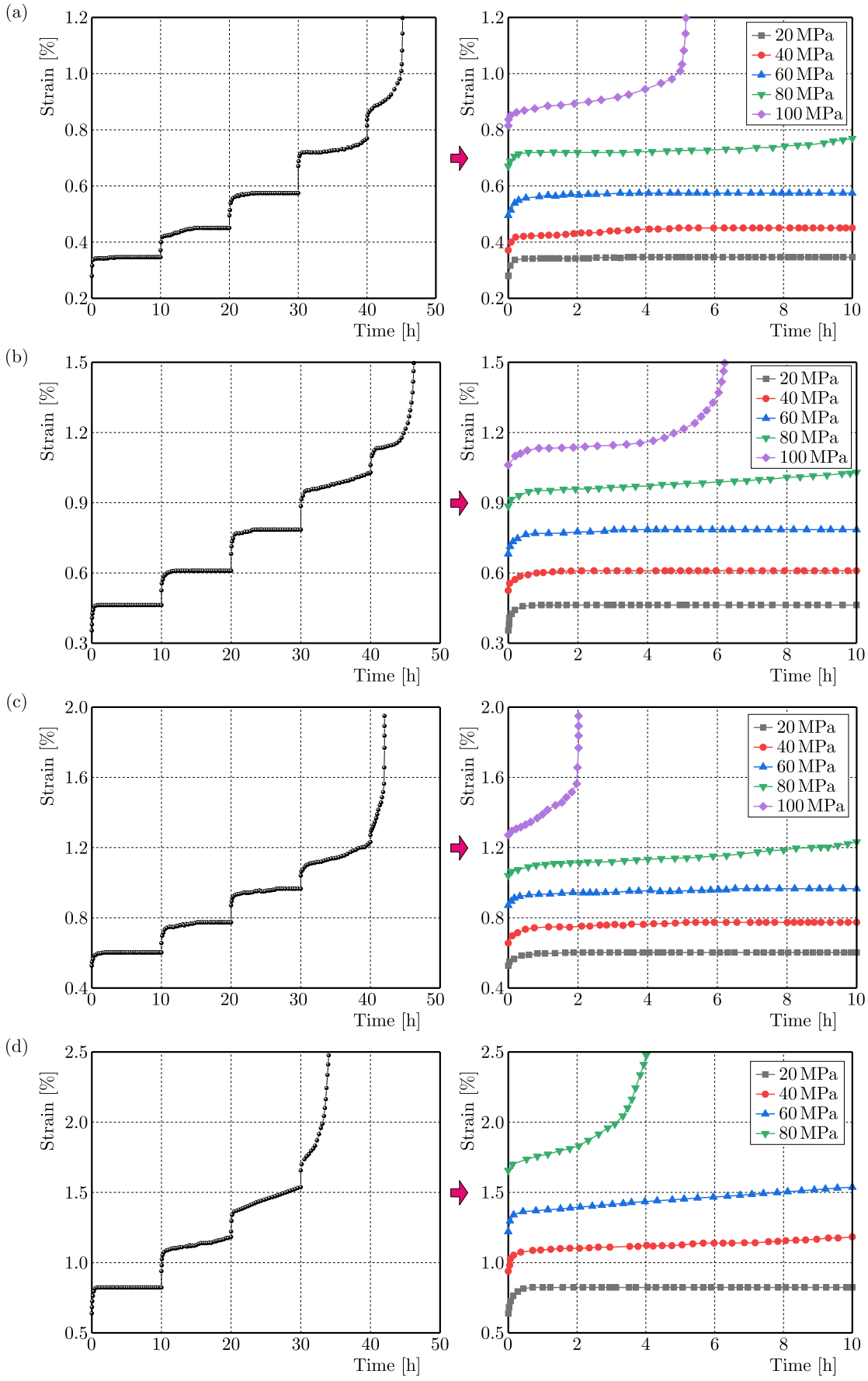

Fig. 3. Creep curve of granite under different water content after high temperature cooling: (a) $M = 0\,\%$; (b) $M = 0.5\,\%$; (c) $M = 1.0\,\%$; (d) $M = 2.0\,\%$.

With the increase of water content, the bonding between the particles inside the specimen gradually weakens, resulting in the decline of the specimen's resistance to external loads, which is reflected in the gradual increase of the peak strain of granite. It is worth explaining that when the water content reaches the state of full water, the granite specimen will be destroyed at the medium stress level. This further shows that the failure of the specimen is closely related to the water content.

3.2. Creep rate

Creep rate is an index to measure the creep deformation speed of rock, and represents the change rate of rock creep deformation with time. According to the changing trend, the creep rate curve can be divided into three stages under the constant stress: decelerating creep rate, steady creep rate and accelerating the creep rate. When $M = 0\,\%$, the curve belongs to the typical three-stage change, while the creep rate curve under other water content is more complicated (Fig. 4). In the deceleration creep rate stage, the creep rate decreases from the highest value to 0 in a very short time, which is mainly the result of the resistance of the internal adhesion of the specimen to the external load. As the internal stress and external load gradually tend to be stable, the corresponding creep rate curve is also maintained at about 0. With the increase of stress level, two stages of decay creep rate and stable creep rate repeatedly appear in the creep rate curve. When the specimen reaches the final failure stress, the appearance of instantaneous macroscopic failure indicates that the specimen has a large displacement and

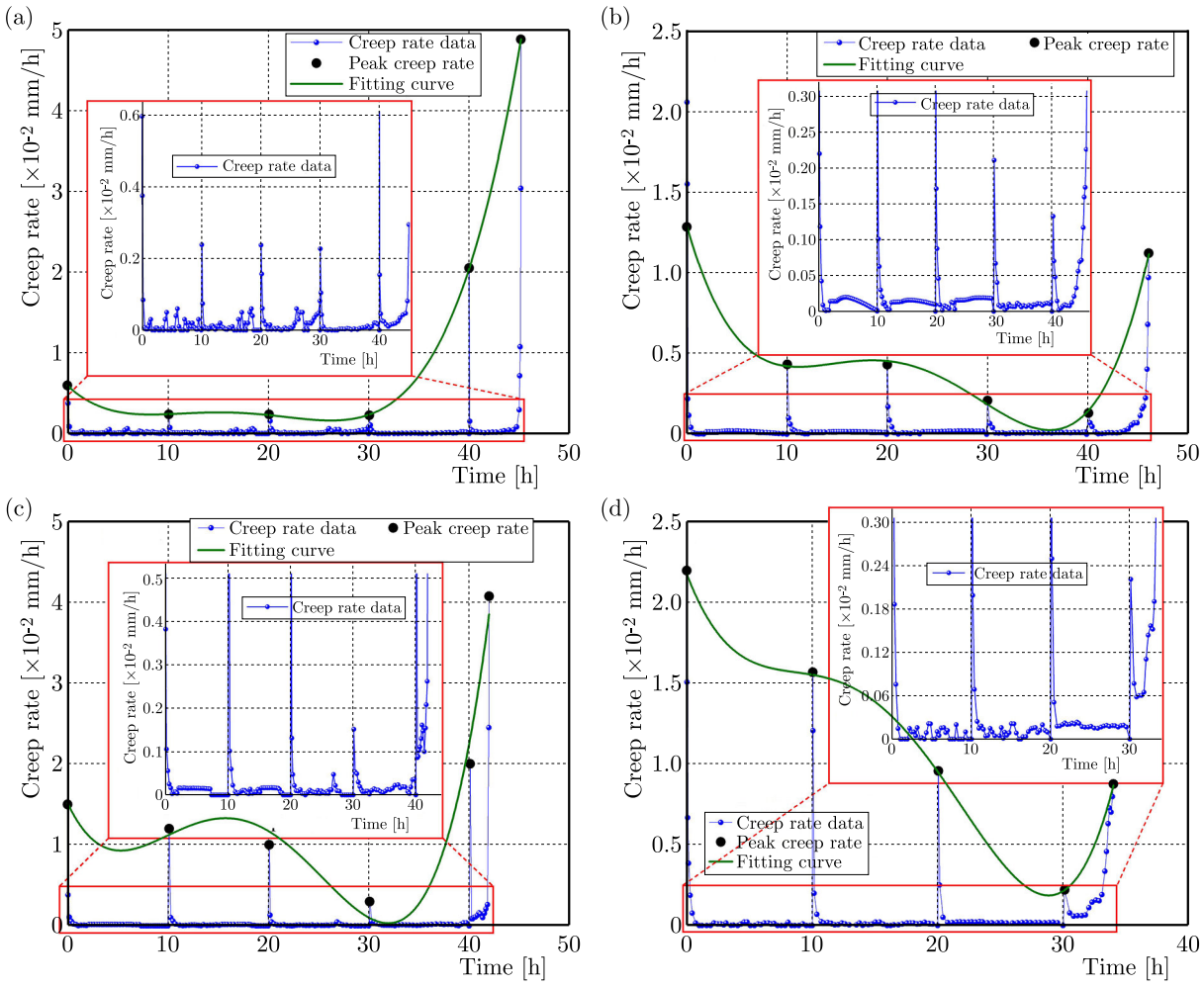

Fig. 4. Creep rate of granite under different water content after high temperature cooling: (a) $M = 0\,\%$; (b) $M = 0.5\,\%$; (c) $M = 1.0\,\%$; (d) $M = 2.0\,\%$.

deformation in a short time, which is manifested as a large increase in creep rate. This stage is called the accelerated creep rate.

In addition, the maximum local strain rate is different in the decay stage under different stress levels. Through fitting, it is found that the variation trend satisfies the polynomial function (Table 1). This further shows that the creep deformation curve of granite is related to the stress level and satisfies a certain function change law.

Table 1. Fitting results of creep rate curve.

Water content [%]	$d\varepsilon/dt = A_0 + A_1 \times t + A_2 \times t^2 + A_3 \times t^3 + A_4 \times t^4$					R^2
	A_0	A_1	A_2	A_3	A_4	
$M = 0$	0.60	−0.12	0.01	-5.86×10^{-4}	8.85×10^{-6}	0.999
$M = 0.5$	1.29	−0.21	0.02	-6.26×10^{-4}	7.12×10^{-6}	0.993
$M = 1.0$	1.51	−0.26	0.04	1.74×10^{-3}	2.50×10^{-5}	0.910
$M = 2.0$	2.17	−0.20	0.03	-1.37×10^{-3}	2.23×10^{-5}	0.996

3.3. Failure mode of specimens

Figure 5 shows the failure characteristics and fracture modes of granite under different water content. In dry environment, granite has typical brittleness characteristics, and the fracture mode is mainly tensile fracture. With the expansion and development of secondary cracks at the end of the specimen and the main tensile crack, the overall integrity of the granite specimen is good. The reason is that under the action of high temperature, the internal water content of granite is 0, the cementation between specimen particles is increased, and high temperature can improve the thermal expansion effect of rock particles. In the natural state, the fracture expansion of granite is mainly of tensile type, and some shear types appear in the micro-fracture concentration area, which may be due to the fracture of the internal crack of the specimen due to water erosion under the natural state, and the stress concentration phenomenon of the crack tip is intensified by the external load.

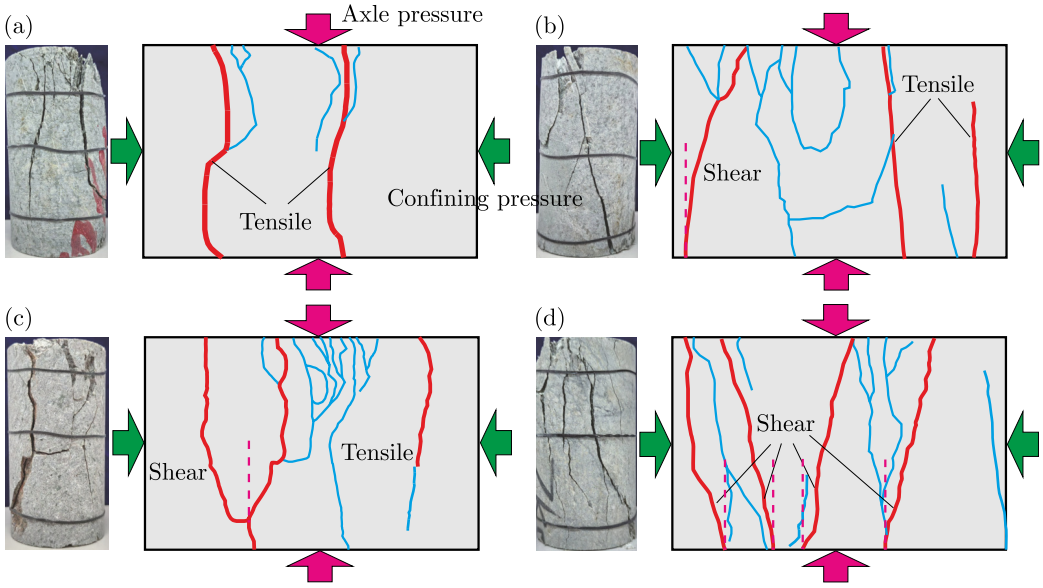

Fig. 5. Compressive failure modes of granite with different water content after high temperature cooling.

When the specimen is subjected to triaxial compression under naturally saturated water, the corresponding failure mode changes from tensile under low water content to shear under high

water content. The shear crack is approximately "Y" type and accompanied by the appearance of concentrated micro-cracks, while the tensile crack, as a secondary crack, fails to penetrate the specimen axially. Finally, the failure mode of the specimen in the fully saturated state is shear fracture, and the fracture degree of the specimen is the highest, which indicates that the cementation between the specimen particles attenuates the fastest under the high water content, and the secondary cracks can penetrate the specimen.

4. Damage creep model

4.1. Damage state variable

In this study, the damage mainly includes thermal expansion damage caused by high temperature cooling, microfissure expansion damage caused by different water conditions, and coupling damage caused by two factors under load.

(1) Temperature damage: the degradation effect of temperature on rock is mainly manifested in two aspects. First, the thermal stress generated by the temperature increase is applied to the internal structure of rock, resulting in the increase of micropore cracks. Second, the increase of temperature changes the arrangement structure of crystals or particles inside the rock, which is manifested as a softening of mechanical properties. Therefore, the temperature damage can be defined by the ratio of rock elastic modulus under different temperatures (Pudasaini & Krautblatter, 2021):

$$D = 1 - \frac{\sigma_T}{\sigma_0}, \tag{4.1}$$

where σ_T and σ_0 are the peak stress of the rock after high temperature and normal temperature (22°), respectively.

It can be seen from the previous analysis that the elastic modulus is related to temperature. Therefore, the elastic modulus is selected as the thermal damage variable in this study to describe the influence of temperature on rock bearing performance, and the thermal damage variable generated by temperature is defined as (Fig. 6)

$$D_T = aT^3 + bT^2 + cT + d, \tag{4.2}$$

where a, b, c, and d are equation coefficients.

(2) Water content damage: under the influence of different water content, pores and cracks in the rock mass expand and penetrate under the action of repeated frost heave, forming more holes and hindering the propagation of P-wave. The wave velocity decreases gradually with the increase of water content, which indicates that the rock sample structure tends to be stable gradually (Shukla *et al.*, 2009). Therefore, the longitudinal wave velocity can be used to characterize the rock damage characteristics under different water content:

$$D_p = 1 - \frac{P_w}{P_0}, \tag{4.3}$$

where P_w is the longitudinal wave velocity of the rock under different water content, P_0 is the longitudinal wave velocity of the dry specimen. Taking the elastic modulus of granite as the damage variable, the damage variable of the elastic modulus of rock under the action of water was obtained as follows (Singh *et al.*, 2018):

$$D_e = 1 - \frac{E_w}{E_0}, \tag{4.4}$$

where E_w is the elastic modulus of the specimen under different water content, and E_0 is the elastic modulus of the dry specimen.

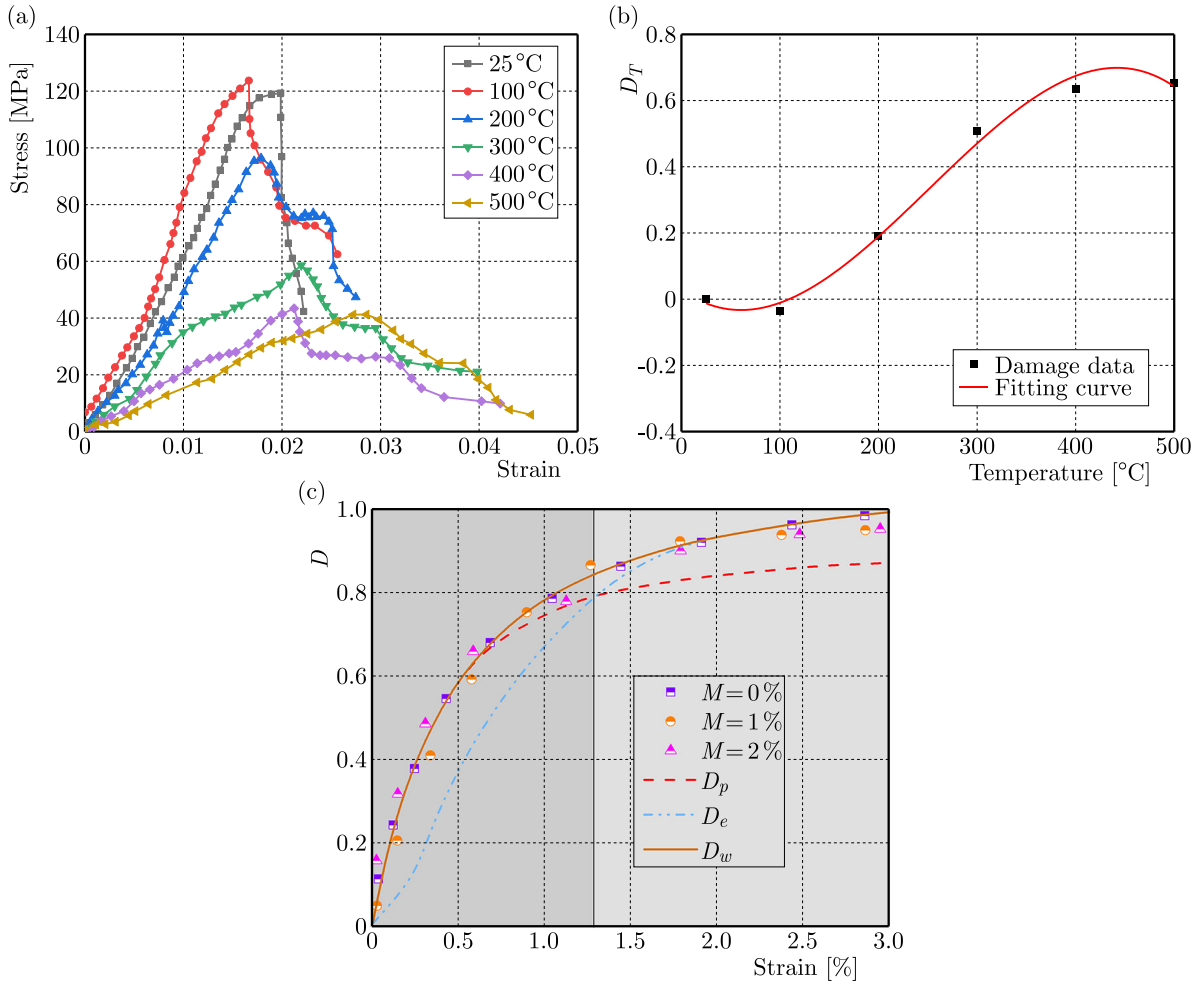

Fig. 6. (a) Stress-strain curves of granite at different temperatures; (b) temperature damage variable curve; (c) granite damage variable curve under different water content.

As a damage variable, the longitudinal wave velocity can only be used to gauge the change of the physical properties of the rock. Similarly, the elastic modulus in the mechanical properties of the rock as a damage variable index lacks the macroscopic physical properties of the specimen, and there are errors in the characterization of the damage variables by the two factors (Fig. 6c). Among them, the damage variable of wave velocity can only reflect the characteristics of the damage variable at the early stage, while the damage variable of elastic modulus mainly represents the damage variable at the later stage. Therefore, this study combines two factors to construct a new type of damage variable:

$$D_w = \xi D_p + \psi D_e = \xi \left(1 - \frac{P_w}{P_0}\right) + \psi \left(1 - \frac{E_w}{E_0}\right), \tag{4.5}$$

where ζ and ψ are water content damage parameters. The new water content damage variable can better reflect the variation trend of damage variable under the low stress level and the high stress level.

(3) Coupled damage variables: according to the extended strain equivalence principle, the damage caused by a high temperature is taken as the first damage state, and the total damage caused by a high temperature and water content is taken as the second damage state. Then the damage constitutive relationship of rock mass after high temperature cooling can be expressed as follows (Weibull, 1951):

$$\sigma_1 = E_0\varepsilon_1(1-D) + \mu(\sigma_2+\sigma_3),$$
$$\sigma_2 = E_0\varepsilon_2(1-D) + \mu(\sigma_1+\sigma_3), \tag{4.6}$$
$$\sigma_3 = E_0\varepsilon_3(1-D) + \mu(\sigma_1+\sigma_2),$$

where σ_i and ε_i are principal nominal stress and nominal strain; E_0 is the elastic modulus of intact rock; μ is Poisson's ratio of rock mass; D is the total damage variable of rock mass. It is assumed that N, N_T, N_w, N_1, and N_2 are the total number of microelements, the number of high temperature damaged microelements, the number of water damaged microelements, the number of high temperature and water coupled damaged microelements, and the number of undamaged microelements, respectively. High temperature initial damage D_T can be defined as the ratio of the number of high temperature damage particles to the total number of particles:

$$D_T = \frac{N_T}{N}. \tag{4.7}$$

Rock mass is further damaged under the action of different water content, and the load damage variable D_w of rock mass is defined as

$$D_w = \frac{N_w - N_1}{N - N_T}. \tag{4.8}$$

The final damage degree of rock mass is defined as the total damage variable D of rock mass with different water content under high temperature cooling:

$$D = \frac{N_w - N_1 + N_T}{N}. \tag{4.9}$$

Bring Eqs. (4.2), (4.5), (4.7), and (4.8) into Eq. (4.9) to get:

$$D = D_T + D_w - D_wD_T = D_T + (1-D_T)D_w = (aT^3 + bT^2 + cT + d) + (1 - aT^3 - bT^2 - cT - d)\left[\xi\left(1 - \frac{P_w}{P_0}\right) + \psi\left(1 - \frac{E_w}{E_0}\right)\right]. \tag{4.10}$$

4.2. Coupling damage model

4.2.1. Burgers model and accelerate body

(1) The Burgers model (Fig. 7a): the constitutive equation of the Burgers model can be obtained as follows:

$$\sigma_0 + \left(\frac{\eta_1}{E_0} + \frac{\eta_1\eta_2}{E_1}\right)\dot{\sigma}_0 + \frac{\eta_1\eta_2}{E_0E_1}\ddot{\sigma}_0 = \eta_1\dot{\varepsilon} + \frac{\eta_1\eta_2}{E_1}\ddot{\varepsilon}, \tag{4.11}$$

where σ_0 and ε are the total stress and strain of the model; E_i and η_i are the elastic and viscosity parameters, respectively.

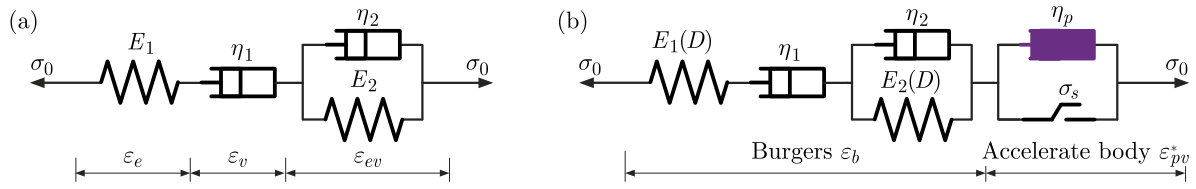

Fig. 7. (a) Schematic diagram of the Burgers model components; (b) schematic diagram of optimizing the Burgers model based on damage variables.

The total axial stain of the Burgers model includes elastic, viscous, and elastoviscous bodies:

$$\varepsilon = \varepsilon_e + \varepsilon_v + \varepsilon_{ve}. \tag{4.12}$$

The Laplace transform of Eq. (4.12) is obtained (Davies *et al.*, 2000):

$$\widetilde{\varepsilon}_e(s) + \widetilde{\varepsilon}_v(s) + \widetilde{\varepsilon}_{ve}(s) = \frac{\sigma_0}{E_1 s} + \frac{\sigma_0}{\eta_1 s^2} + \frac{\sigma_0}{(E_2 + \eta_2 s)s}, \tag{4.13}$$

where $\widetilde{\varepsilon}$ is the Laplace variation of ε and s is the complex variable of the Laplace transform space.

Applying the inverse Laplace transformation to Eq. (4.13), the creep equation of the Burgers model can be calculated by:

$$\varepsilon = \frac{\sigma_0}{E_1} + \frac{\sigma_0}{\eta_1} t + \frac{\sigma_0}{E_2}\left[1 - \exp\left(-\frac{E_2}{\eta_2} t\right)\right]. \tag{4.14}$$

(2) The accelerate body: the nonlinear acceleration element essentially describes the macroscopic displacement of rock, and the microscopic manifestation of the macroscopic displacement is the compaction, expansion and development of micro-cracks, and the expansion of micro-cracks is controlled by external loads. Therefore, the nonlinear accelerating body is closely related to the external load, and the content of the specimen under the low stress load mainly shows the compaction and slow expansion of micro-cracks, while the rapid expansion of micro-cracks under the high stress level gradually changes into macroscopic cracks. The deformation rate of the nonlinear accelerating element per unit time shows a nonlinear change characteristic, which belongs to the exponential function series. The constitutive equation of the viscosity coefficient evolution of the nonlinear accelerating element with time is defined as (Fig. 7b):

$$\dot{\varepsilon} = \frac{\eta_p}{p} \exp^{pt}, \tag{4.15}$$

where η_p and p are the accelerate body parameters. Therefore, the nonlinear acceleration element was controlled by the critical stress σ_s, and the corresponding creep equation is as follows:

$$\varepsilon = \begin{cases} 0 & (\sigma_0 \le \sigma < \sigma_s), \\ \dfrac{\sigma - \sigma_s}{\eta_p} \exp^{pt} & (\sigma \ge \sigma_s), \end{cases} \tag{4.16}$$

where σ_s is the long-term strength.

4.2.2. Damage model

The corresponding constitutive equation is as follows:

$$\frac{\ddot{\sigma}}{E_1(1-D)} + \left(\frac{1}{\eta_2} + \frac{E_2}{E_1\eta_2} + \frac{1}{\eta_1} + \frac{pe^{pt}}{\eta_p}\right)\dot{\sigma} + \left(1 + \frac{E_2}{\eta_2}\right)\frac{pe^{pt}}{\eta_p}(\sigma - \sigma_s) + \frac{E_2}{\eta_2}\int \frac{pe^{pt}}{\eta_p}(\sigma - \sigma_s)\,\mathrm{d}t = \frac{E_2}{\eta_2}\dot{\varepsilon} + \ddot{\varepsilon}. \tag{4.17}$$

Based on the above relation, we can derive a creep equation of the damage model:

– when $\sigma_0 \le \sigma < \sigma_s$, the damage model is transformed into the Burgers model to describe the decay and steady stages of the rock:

$$\varepsilon = \frac{\sigma_0}{E_1(1-D)} + \frac{\sigma_0}{\eta_1} t + \frac{\sigma_0}{E_2(1-D)}\left[1 - \exp\left(-\frac{E_2}{\eta_2} t\right)\right], \tag{4.18}$$

– when $\sigma \geq \sigma_s$, the damage model can describe the whole creep stage of the specimen:

$$\varepsilon = \frac{\sigma_0}{E_1(1-D)} + \frac{\sigma_0}{\eta_1}t + \frac{\sigma_0}{E_2(1-D)}\left[1 - \exp\left(-\frac{E_2}{\eta_2}t\right)\right] + \frac{\sigma - \sigma_s}{\eta_p}\exp^{pt}. \tag{4.19}$$

The compression test of granite with different water content under high temperature cooling meets the three-way stress state, which accords with the actual engineering state. Therefore, the three-dimensional damage constitutive model of granite with different water content is shown as follows:

$$\varepsilon_i = \begin{cases} \frac{\sigma_1+2\sigma_3}{9K} + \frac{\sigma_1-\sigma_3}{3G_1(1-D)} + \frac{\sigma_1-\sigma_3}{3\eta_1}t + \frac{\sigma_1-\sigma_3}{3G_2(1-D)}\left[1 - \exp\left(-\frac{G_2}{\eta_2}t\right)\right] & (\sigma < \sigma_s), \\ \frac{\sigma_1+2\sigma_3}{9K} + \frac{\sigma_1-\sigma_3}{3G_1(1-D)} + \frac{\sigma_1-\sigma_3}{3\eta_1}t + \frac{\sigma_1-\sigma_3}{3G_2(1-D)}\left[1 - \exp\left(-\frac{G_2}{\eta_2}t\right)\right] + \frac{\sigma_1-\sigma_3-\sigma_s}{\eta_p}e^{pt} & (\sigma \geq \sigma_s). \end{cases} \tag{4.20}$$

4.3. Model validation analysis

Combined with the creep test results of granite under different water content after high temperature cooling, the L-M nonlinear optimization algorithm was adopted to optimize and fit the material parameters by using the optimization software 1stOpt, and the parameters of the nonlinear damage constitutive model in this study were obtained.

Figure 8 shows the comparison of the test and fitting results of granite creep curve under different water content. It can be seen from the figure that the prediction results of damage

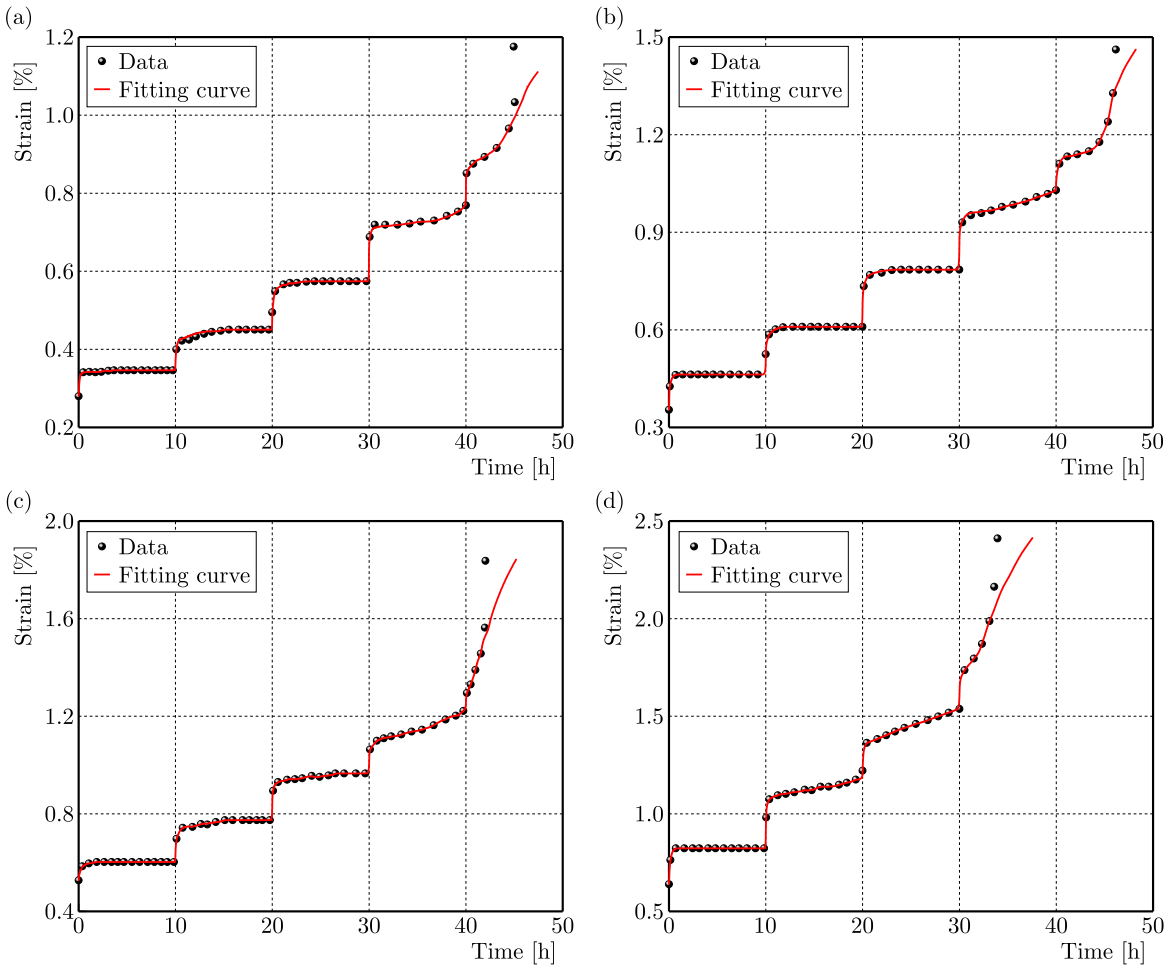

Fig. 8. Fitting curves under different water content:
(a) $M = 0\,\%$; (b) $M = 0.5\,\%$; (c) $M = 1.0\,\%$; (d) $M = 2.0\,\%$.

creep model are consistent with the general trend of test results, which can reflect the creep characteristics of granite. At the same time, there is a certain degree of error between the fitting results and the test results, but the error between them is relatively small, which indicates the accuracy of the prediction results of the model.

5. Discussion

The creep deformation and failure process of granite with different moisture content under high temperature cooling is essentially a thermal (temperature) → flow (water) → solid (rock) coupling problem (Fig. 9). First, water transfers heat in the form of thermal convection, while temperature transfers high temperature to water supply through the thermal conduction effect. Secondly, based on the theory of thermal expansion, high temperature applies thermal stress to the rock, while granite stores the heat under temperature action in the form of strain energy in the specimen (Pathiranagei & Gratchev, 2022). Then the water flows into the micro-pores and micro-cracks, and the micro-cracks of the samples are cracked under the action of external loads, while the micro-cracks of the rock samples are characterized by the crack opening and porosity.

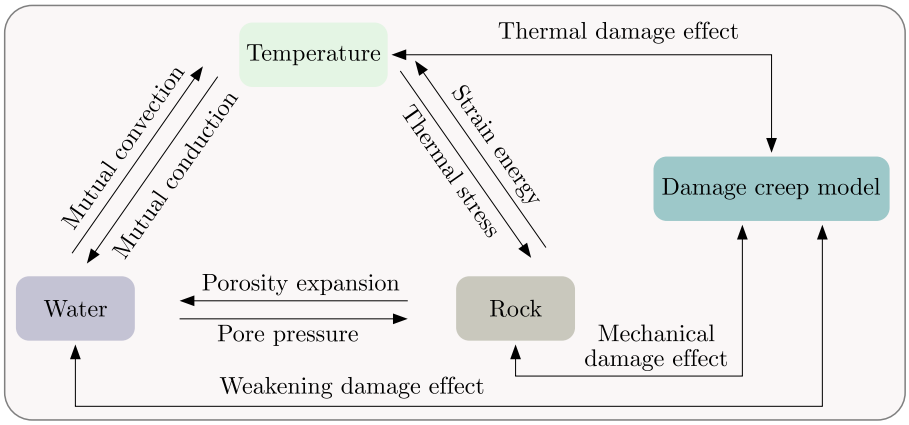

Fig. 9. Coupling schematic diagram of rock, water, and temperature.

Finally, temperature, water and rock together constitute the damage creep model, in which temperature is connected to the damage model through the thermal damage effect, water influences the creep model by weakening the damage effect, and rock specimens feedback the constitutive model through the mechanical damage effect. Specifically, the effect of water content on the mechanical properties of granite is mainly reflected in the peak stress, peak strain and elastic modulus. Figure 10 shows the variation of peak stress, peak strain and elastic modulus of granite samples with water content.

The peak stress of granite samples has a good linear relationship with water content, and the peak stress decreases with the increase of water content. This is because the water content will further increase the proportion of water in the pores of the specimen, and the cementation between granite particles will be gradually eroded, resulting in a decline in the resistance to external loads, and thus a downward trend in the peak stress. The peak strain of granite samples increases with the increase of water content, and its linear characteristics are obvious, which indicates that the increase of water content can improve the plastic characteristics of rock. From the perspective of elastic modulus, with the increase of water content, the elastic modulus presents a decreasing trend, and its decreasing curve conforms to the exponential function, which indicates that the change of water content can affect the mechanical properties of rock, but the influence on the stiffness of rock is non-linear.

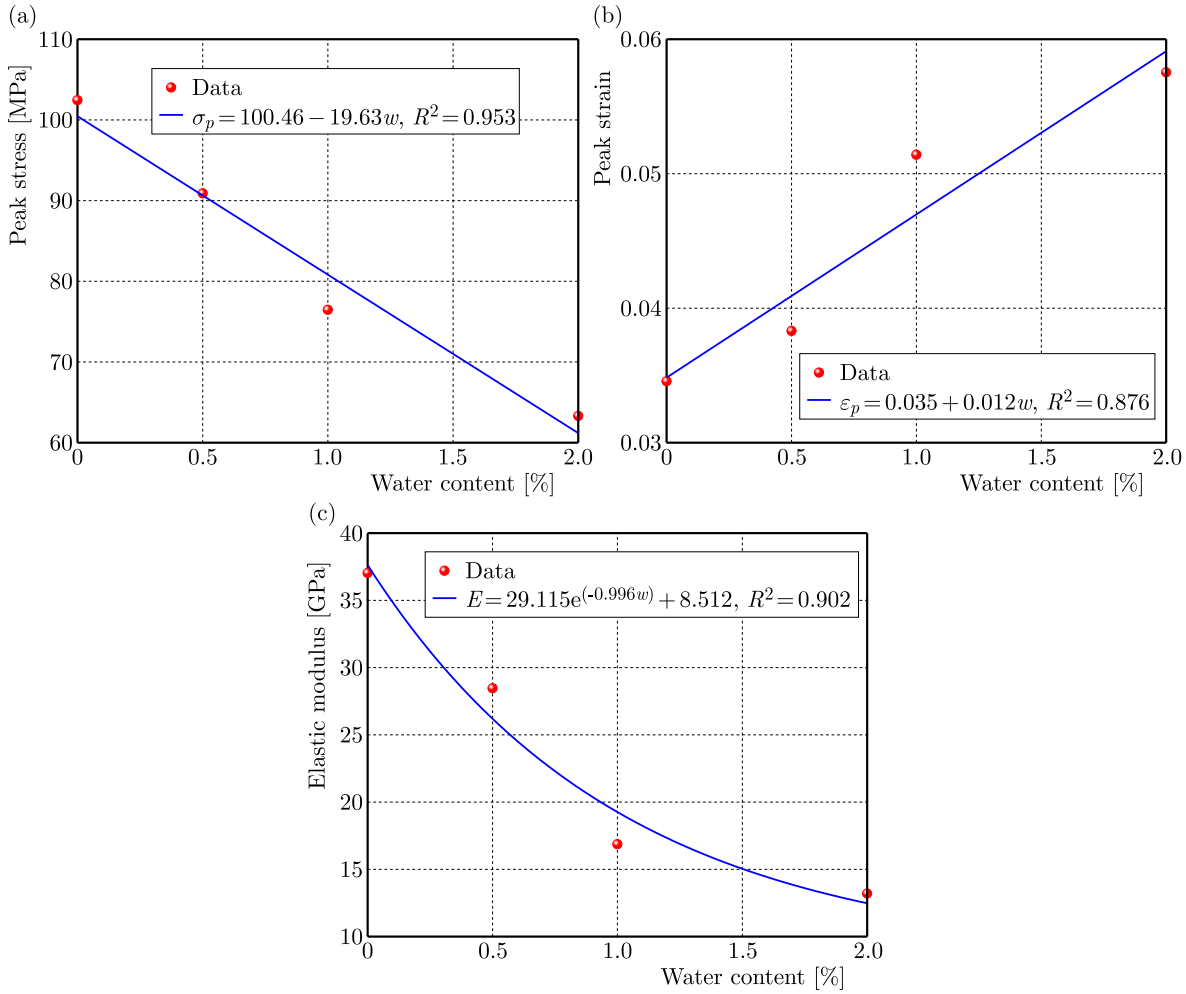

Fig. 10. Curve of mechanical properties of granite with water content: (a) peak stress; (b) peak strain; (c) elastic modulus.

6. Conclusions

Triaxial compression creep tests were carried out on granite at a high temperature and water content, the creep characteristics, failure modes and constitutive models were analyzed. Relevant conclusions are shown as follows:

- the curve of granite with different water content at a high temperature cooling has typical creep characteristics, in which the peak stress gradually decreases with the increase of water content, and the peak strain shows an opposite trend;
- the failure mode of the dry specimen at a high temperature is mainly tensile fracture, and with the increase of water content, the fracture mode changes from tensile crack to shear crack, and the granite in the fully saturated state shows shear failure;
- the damage creep model not only considers the damage factors such as high temperature and water content, but also connects the acceleration element in series. The model can well describe the whole process of creep damage of granite with different water content at a high temperature cooling.

References

1. Abbas, H.A., Mohamed, Z., & Kudus, S.A. (2023). Deformation behaviour, crack initiation and crack damage of weathered composite sandstone-shale by using the ultrasonic wave and the acoustic

emission under uniaxial compressive stress. *International Journal of Rock Mechanics and Mining Sciences*, *170*, Article 105497. https://doi.org/10.1016/j.ijrmms.2023.105497

2. Ahmed, Z., Wang, S., Hashmi, M.Z., Zishan, Z., & Chengjin, Z. (2020). Causes, characterization, damage models, and constitutive modes for rock damage analysis: a review. *Arabian Journal of Geosciences*, *13*(16), Article 806. https://doi.org/10.1007/s12517-020-05755-3

3. Bandis, S.C., Lumsden, A.C., & Barton, N.R. (1983). Fundamentals of rock joint deformation. *International Journal of Rock Mechanics and Mining Sciences & Geomechanics Abstracts*, *20*(6), 249–268. https://doi.org/10.1016/0148-9062(83)90595-8

4. Cao, H., Zhu, D., Bao, T., Sun, P., Li, J., & Erneste, H. (2024). Applicability of rock damage model based on power law distribution. *Acta Geophysica*, *72*(5), 3021–3036. https://doi.org/10.1007/s11600-023-01260-9

5. Davies, M.C.R., Hamza, O., Lumsden, B.W., & Harris, C. (2000). Laboratory measurement of the shear strength of ice-filled rock joints. *Annals of Glaciology*, *31*, 463–467. https://doi.org/10.3189/172756400781819897

6. Diederichs, M.S., Kaiser, P.K., & Eberhardt, E. (2004). Damage initiation and propagation in hard rock during tunnelling and the influence of near-face stress rotation. *International Journal of Rock Mechanics and Mining Sciences*, *41*(5), 785–812. https://doi.org/10.1016/j.ijrmms.2004.02.003

7. Gao, W., Chen, X., Hu, C., Zhou, C., & Cui, S. (2020). New damage evolution model of rock material. *Applied Mathematical Modelling*, *86*, 207–224. https://doi.org/10.1016/j.apm.2020.05.002

8. Hamdi, E., Romdhane, N.B., & Le Cléac'h, J.M. (2011). A tensile damage model for rocks: Application to blast induced damage assessment. *Computers and Geotechnics*, *38*(2), 133–141. https://doi.org/10.1016/j.compgeo.2010.10.009

9. Lemaitre, J. (1985). A continuous damage mechanics model for ductile fracture. *Journal of Engineering Materials and Technology*, *107*(1), 83–89. https://doi.org/10.1115/1.3225775

10. Lin, H., Feng, J., Cao, R., & Xie, S. (2022). Comparative analysis of rock damage models based on different distribution functions. *Geotechnical and Geological Engineering*, *40*(1), 301–310. https://doi.org/10.1007/s10706-021-01899-5

11. Liu, G., Huang, X., & Pang, J. (2020a). The uniaxial creep characteristics of red sandstone under dry-wet cycles. *Advances in Civil Engineering*, *2020*(1), Article 8841773. https://doi.org/10.1155/2020/8841773

12. Liu, L., Ji, H., Elsworth, D., Zhi, S., Lv, X., & Wang, T. (2020b). Dual-damage constitutive model to define thermal damage in rock. *International Journal of Rock Mechanics and Mining Sciences*, *126*, Article 104185. https://doi.org/10.1016/j.ijrmms.2019.104185

13. Pathiranagei, S.V. & Gratchev, I. (2022). Coupled thermo-mechanical constitutive damage model for sandstone. *Journal of Rock Mechanics and Geotechnical Engineering*, *14*(6), 1710–1721. https://doi.org/10.1016/j.jrmge.2022.02.010

14. Peellage, W.H., Fatahi, B., & Rasekh, H. (2024). Stiffness and damping characteristics of jointed rocks under cyclic triaxial loading subjected to prolonged cyclic loading. *International Journal of Fatigue*, *181*, Article 108121. https://doi.org/10.1016/j.ijfatigue.2023.108121

15. Pudasaini, S.P. & Krautblatter, M. (2021). The mechanics of landslide mobility with erosion. *Nature Communications*, *12*, Article 6793. https://doi.org/10.1038/s41467-021-26959-5

16. Ranjith, P.G., Viete, D.R., Chen, B.J., & Perera, M.S.A. (2012). Transformation plasticity and the effect of temperature on the mechanical behaviour of Hawkesbury sandstone at atmospheric pressure. *Engineering Geology*, *151*, 120–127. https://doi.org/10.1016/j.enggeo.2012.09.007

17. Shao, J., Zhang, W., Wu, X., Lei, Y., & Wu, X. (2022). Rock damage model coupled stress–seepage and its application in water inrush from faults in coal mines. *ACS Omega*, *7*(16), 13604–13614. https://doi.org/10.1021/acsomega.1c07087

18. Shukla, S.K., Gupta, S.K., & Sivakugan, N. (2009). Active earth pressure on retaining wall for c-ϕ soil backfill under seismic loading condition. *Journal of Geotechnical and Geoenvironmental Engineering*, *135*(5), 690–696. https://doi.org/10.1061/(ASCE)GT.1943-5606.0000003

19. Singh, A., Kumar, C., Kannan, L.G., Rao, K.S., & Ayothiraman, R. (2018). Estimation of creep parameters of rock salt from uniaxial compression tests. *International Journal of Rock Mechanics and Mining Sciences*, *107*, 243–248. https://doi.org/10.1016/j.ijrmms.2018.04.037

20. Weibull, W. (1951). A statistical distribution function of wide applicability. *Journal of Applied Mechanics*, *18*(3), 293–297. https://doi.org/10.1115/1.4010337

Manuscript received September 3, 2024; accepted for publication February 18, 2025; published online April 24, 2025.